Commun Nonlinear Sci Numer Simulat xxx (2015) xxx–xxx

Contents lists available at ScienceDirect

Commun Nonlinear Sci Numer Simulat

journal homepage: www.elsevier.com/locate/cnsns

Mixed-mode synchronization between two inhibitory neurons with post-inhibitory rebound

Roman Nagornov[a,*], Grigory Osipov[a], Maxim Komarov[a,b,c], Arkady Pikovsky[b], Andrey Shilnikov[a,d]

[a] Institute for Information Technologies, Mathematics and Mechanics, Nizhni Novgorod State University, Gagarin Av. 23, 606950 Nizhni Novgorod, Russia
[b] Department of Physics and Astronomy, University of Potsdam, Karl-Liebknecht-Str 24/25, Potsdam, Germany
[c] University of California, Riverside, 900 University Ave., Riverside, CA 92521, USA
[d] Neuroscience Institute and Department of Mathematics and Statistics, Georgia State University, 100 Piedmont Str., Atlanta, GA 30303, USA

ARTICLE INFO

Article history:
Received 17 May 2015
Revised 4 November 2015
Accepted 28 November 2015
Available online xxx

Keywords:
Synchronization
Hodgkin–Huxley model
Half-center oscillator
Post-inhibitory rebound

ABSTRACT

We study an array of activity rhythms generated by a half-center oscillator (HCO), represented by a pair of reciprocally coupled neurons with post-inhibitory rebounds (PIR). Such coupling-induced bursting possesses two time scales, one for fast spiking and another for slow quiescent periods, is shown to exhibit an array of synchronization properties. We discuss several HCO configurations constituted by two endogenous bursters, by tonic-spiking and quiescent neurons, as well as mixed-mode configurations composed of neurons of different type. We demonstrate that burst synchronization can be accompanied by complex, often chaotic, interactions of fast spikes within synchronized bursts.

© 2015 Published by Elsevier B.V.

1. Introduction

Synchronization of coupled oscillators is a fundamental phenomenon in nonlinear systems that has been observed in a wide range of diverse applications [1]. The mathematical concept of synchronization [2], first introduced and developed for periodic oscillators has been further generalized for other aperiodic systems, including ones with chaotic dynamics. In life sciences, of a keen interest is synchronization or phase locking among oscillators with multiple time scales. They may include mixed-mode and slow–fast relaxation-type oscillators [3], whose interaction can give rise to the onset of a variety of synchronization patterns [4–7]. In neuroscience, a plethora of rhythmic motor behaviors with diverse time scales, such as heartbeat, respiration, chewing, and locomotion on land and in water are produced and governed by neural networks called Central Pattern Generators (CPGs) [8,9]. The CPG is a microcircuit of neurons that is able to autonomously generate an array of polyrhythmic bursting patterns, underlying various motor behaviors.

Endogenous (self-sustained) bursting and network (coupling-induced) bursting are composite oscillatory behaviors, featuring active phases during which a neuron or a group of neurons generates trains of fast action potentials, which are alternated with long interburst intervals during which it remains inactive or quiescent, until a new cycle of bursting occurs. In this paper we examine synchronization of bursting patterns emerging through interactions of two interneurons coupled reciprocally by fast inhibitory synapses. This study has been driven by two major motivations: first, a general one concerning questions on

* Corresponding author. Tel.: +79040538156.
E-mail address: nagornov.r@gmail.com (R. Nagornov).

http://dx.doi.org/10.1016/j.cnsns.2015.11.024
1007-5704/© 2015 Published by Elsevier B.V.

Please cite this article as: R. Nagornov et al., Mixed-mode synchronization between two inhibitory neurons with post-inhibitory rebound, Commun Nonlinear Sci Numer Simulat (2015), http://dx.doi.org/10.1016/j.cnsns.2015.11.024

UNCORRECTED PROOF

synchronization of mixed-mode oscillators. The second is a neuroscience related one, aimed at a progress in understanding of intrinsic mechanisms of rhythmogenesis in CPGs, composed, often symmetrically, of such small networks of interneurons, as outlined below. It is still unclear how CPGs can achieve the level of synergy, flexibility, and robustness to produce a plethora of rhythmic patterns observed in nature.

Recent experimental and theoretical studies have disclosed a distinct role of CPGs in generation of adaptive and coordinated motor activity of animals [9–12]. An important feature of CPGs is their ability to produce various types of rhythmic bursting activity, what causes flexible and adaptive locomotion of an organism. To robustly govern motor patterns, CPGs are in a position to flexibly adjust their oscillatory properties (such as bursts duration, frequency of spiking, phase relations of bursts) due to a feedback from sensory inputs, for example, in response to changes of an environment [9,10]. Up to a certain extent, the flexibility of CPG behaviors may be attributed to its multistability (of several coexistent attractors representing different bursting rhythms in a phase space of the dynamical system) allowing for fast switching between operating modes [7,13].

From the theoretical point of view, a CPG is modeled as a small network of coupled oscillatory, or quiescent, interneurons, each described by a system of nonlinear ordinary differential or difference equations (dynamical system) [11,14,15]. The study of CPGs allows one to progress in a general understanding of synchronization patterns in mixed-mode oscillators, applicable to systems of various physical and biological origin.

There is a growing body of experimental evidence that a universal building block of most identified CPGs is a half-center oscillator (HCO) [16]. A HCO is a pair of reciprocally inhibitory interneurons bursting in alternation. Such a pair can be comprised of endogenously bursting interneurons, as well as of intrinsically tonic spiking or quiescent interneurons that start anti-phase bursting only when they are coupled. Theoretical studies [17–21] have indicated that the formation of an anti-phase bursting rhythm is always based on some slow-time-scale dynamics. In the biophysically plausible models, the slow dynamics is firmly associated with the slow membrane currents, such as persistent sodium or slow calcium-dependent current (e.g., potassium after-hyperpolarization current [25]); following [22] we term currents associated with slow-varying concentrations and gating variables as slow ones. There are three basic mechanisms to generate alternating bursting in the HCO: release, escape, and post-inhibitory rebound (PIR). The first mechanism is typical for endogenously bursting neurons [4,6,23]. The other two mechanisms underlie coupling-induced bursting in HCOs comprised of neurons, which are initially depolarized or hyperpolarized quiescent in isolation [9,18,20,24–26].

The PIR mechanism uses reciprocal inhibition to maintain coupling-induced bursting in otherwise hyperpolarized quiescent neurons. As such, either neuron of the HCO must receive a sufficiently strong pulse of some external negative current that initiates the chain reaction in the coupled neurons. PIR triggers an onset of a single or a series of action potentials in the post-synaptic neuron after it has been prolongedly hyperpolarized and abruptly released from inhibition generated by the pre-synaptic neuron during an active, tonic spiking phase of bursting. After that, the neurons of the HCO swap their opposite roles to repeat the PIR mechanism. PIR promotes the action potential generation after a period of sufficiently strong hyper-polarizing (inhibiting) input, as illustrated in Fig. 2. PIR is often caused by a low-threshold activated calcium current in neurons and their biophysically plausible models.

Formation of the antiphase dynamics in inhibitory coupled neurons forming homogeneous HCOs has been extensively studied in Refs. [17–19,21,27] where the primary scope is focused on the dynamics of *identical* neurons, which are either intrinsically excitable or tonically spiking neurons represented by phenomenologically reduced models. Much is yet unknown about the rhythmogenesis of an anti-phase coupling-induced bursting in heterogeneous HCOs described by biologically plausible models derived within the framework of the Hodgkin–Huxley approach. We focus our study on the properties of the emergent bursting in HCOs comprised of non-identical neurons, demonstrating qualitatively different activity types in isolation, i.e. initially chosen at the opposite sides of the transition thresholds between bursting, tonics-spiking, and quiescent behaviors.

An examination of an set of non-identical neurons gives rise to the following issues: (i) the first one concerns with the dynamical robustness and the structural stability (in the parameter space) of the ensemble dynamics against perturbations in the form of a heterogeneity in the ensemble; (ii) the second problem deals with the phase synchronization of a network of oscillatory units. In the case of strong heterogeneity, one should expect possible emergence of additional dynamical phenomena occurring in the system.

Therefore, in this paper, following and capitalizing on the previous studies of PIR mechanisms in homogeneous networks, we examine how PIR contributes to formation, synchronization and robustness of multiple bursting rhythms in heterogeneous HCOs with inhibitory coupled neurons. We focus our consideration upon the oscillatory dynamics occurring in a heterogeneous setup with slightly non-identical neurons, as well as in various mixed-mode HCOs where constituent neurons are chosen to operate in different dynamical regimes: bursting and tonic spiking, or hyperpolarized quiescence.

In this paper, we employ a modification of the Hodgkin–Huxley-type model introduced in [22] to plausibly describe the PIR mechanism. Depending on its parameters, the model is known to produce an array of generic neuronal activities such as excitable dynamics emerging from a hyperpolarized quiescent state, periodic spiking, and bursting.

First, we will examine the conditions that stably reproduce the PIR mechanism in the neurons. We will argue that the PIR is a pivotal component that promotes an alternating bursting rhythm in the HCO made of intrinsically spiking and excitable neurons. Finally, we will show that the PIR mechanism enhances anti-phase coupling-induced bursting that occurs in a pair of endogenously bursting neurons.

Below in this paper we present different dynamical behaviors in coupled neurons, choosing the following structuring: we first describe the dynamics of lumped neurons, and then separately present studies of pairs with different types of lumped dynamics. So, we arrange the results not according to the resulting behavior of the CPG, but according to the properties of uncoupled

Please cite this article as: R. Nagornov et al., Mixed-mode synchronization between two inhibitory neurons with post-inhibitory rebound, Commun Nonlinear Sci Numer Simulat (2015), http://dx.doi.org/10.1016/j.cnsns.2015.11.024

units. The paper is organized as follows: in Section 2 we introduce the neuronal model, and discuss its dynamical properties in Section 3. Section 4 is focused on synchronization properties of a pair of endogenous bursters, while Section 5 examines anti-phase bursting onset in coupled tonic-spiking neurons. Sections 6 and 7 discuss the PIR-mechanisms of the HCO, and the coupling-induced dynamics of mixed pairs (a tonic spiking and a hyperpolarized quiescent ones, or a tonic spiking and a bursting one), respectively.

2. Basic model

In this study we employ a reduced modification of the conductance-based neuronal model proposed in [22] to model rhythmic activity in the isolated thalamic reticular nucleus. The reduced Hodgkin–Huxley type model is a seven-dimensional system of ODEs calibrated to accurately replicate the dynamics of the transmembrane voltage and of the gating variables of ionic channels. The system contains fast Na^+ and K^+ currents responsible for the spike generation mechanism, along with additional low-threshold activated calcium current I_T, which accounts for the mechanism of voltage post-inhibitory rebound in the model. The basic formulation of the coupled model (full details are given in Appendix A) is the following:

$$\begin{aligned} C_m V_i' &= I_{\text{ext}}^{(i)} - f_i(V_i) - \sum_{j=1, j\neq i}^{N} I_{\text{syn}}(V_i, V_j), \\ f_i(V_i) &= I_{\text{leak}}^{(i)} + I_{\text{Na}}^{(i)} + I_{\text{K}}^{(i)} + I_T^{(i)}, \qquad i = 1, 2. \end{aligned} \tag{1}$$

The variable $V_i(t)$ describes evolution of the membrane potential of the ith neuron. The first two terms on the right-hand side of Eq. (1) govern the intrinsic dynamics of the neuron: $I_{\text{ext}}^{(i)}$ stands for a constant external current applied to the neuron, while term $f_i(V_i)$ represents the sum of intrinsic ionic currents. The sum of synaptic currents $\sum_{j=1, j\neq i}^{N} I_{\text{syn}}(V_i, V_j)$ describes the coupling interactions between the neurons. In this study we assume that synapses are instantaneous and non-delayed as in the most CPG networks, and hence we can model the synaptic currents using the fast-threshold modulation paradigm [28]:

$$I_{\text{syn}}(V_i, V_j) = G \cdot S(V_j - \theta_{\text{syn}}) \cdot (V_i - E_{\text{syn}}). \tag{2}$$

In Eq. (2), G is the maximal conductance of synaptic current flowing from pre-synaptic jth neuron into the post-synaptic ith neuron. For inhibitory coupling we set $E_{\text{syn}} = -80$ mV; the synaptic activity (coupling) function $S(V(j))$ is given by the following Boltzmann function:

$$S(V_j) = \frac{1}{1 + e^{-100(V_j - \theta_{\text{syn}})}}, \tag{3}$$

with the synaptic threshold $\theta_{\text{syn}} = 20$ mV is set at the middle of fast spikes (Fig. 1). It follows from Eqs. (2) and (3) that the synaptic current flowing into the post-synaptic neuron attains a maximum when the voltage of the pre-synaptic neuron remains above the synaptic threshold: $V_j > \theta_{\text{syn}}$, and it vanishes otherwise.

As the most Hodgkin–Huxley models, this neuron system (1) has currents (via gating variables) operating on fast and slow time scales. The dynamics of such slow-fast systems is known to be determined by the geometry of the so-called slow motion manifolds [15,29,30]. In the context of mathematical neuroscience, these manifolds are called tonic spiking and quiescent, as they are made of periodic orbits and equilibria of the system, respectively. For the model under consideration, these manifolds, labelled as M_{lc} and M_{eq}, are shown in a 3D projection on the fast (V, n) and slow, h_T, variables, see Fig. 1. Whenever the neuron produces tonic spiking activity, there is a stable periodic orbit on the cylinder-shaped manifold M_{lc}. When the neuron remains hyperpolarized quiescent, then there is a stable equilibrium state on the low branch (shown by the solid orange curve in Fig. 1, whereas the unstable branch is shown by the dashed curve) of the S-shaped M_{eq} below the knee-point. If there are neither stable equilibria nor tonic-spiking periodic orbits on the corresponding manifolds, then the endogenous neuronal bursting is associated with a stable periodic orbit (blue), which follows the tonic spiking and the quiescent manifolds M_{lc} and M_{eq}, and switches between them. In the case of PIR, a transient of the driven (post-inhibitory) neuron is forced by the driving (pre-synaptic) neuron to make a single route along the "bursting orbit with fast spikes", corresponding to turns around M_{lc}, before it comes back to the stable hyperpolarized state. This (equilibrium) state is geometrically located at the intersection of the bottom branch of M_{eq} with the surface labelled by $h_T' = 0$. This surface is called a slow nullcline: for the voltage values above/below it in the phase space, the slow low-threshold Ca^{2+} current I_T becomes in/activated. The slow motion manifold describing quiescence M_{eq}, and the one describing tonic spiking M_{lc}, were obtained using the parameter continuation technique developed for slow-fast systems in [30]. For computations we used the packages CONTENT and MatCont.

In opposite, I_T is inactivated during the fast spiking phase, when the voltage values remain above the surface $h_T' = 0$, see Fig. 1. The full details of the currents representation are given in Appendix A. More details on critical manifolds and bursting in neuronal models can be found in Refs. [15,29,30].

There are two principal control parameters in this system. The first one is the external current, $I_{\text{ext}}^{(i)}$, that governs the activity type in an isolated, uncoupled neuron. The second parameter is the maximal conductance G of the synaptic current introduced in Eq. (2): it controls the coupling strength. Hence, the constant G is the principle parameter determining the dynamics of the coupled neurons.

Please cite this article as: R. Nagornov et al., Mixed-mode synchronization between two inhibitory neurons with post-inhibitory rebound, Commun Nonlinear Sci Numer Simulat (2015), http://dx.doi.org/10.1016/j.cnsns.2015.11.024

UNCORRECTED PROOF

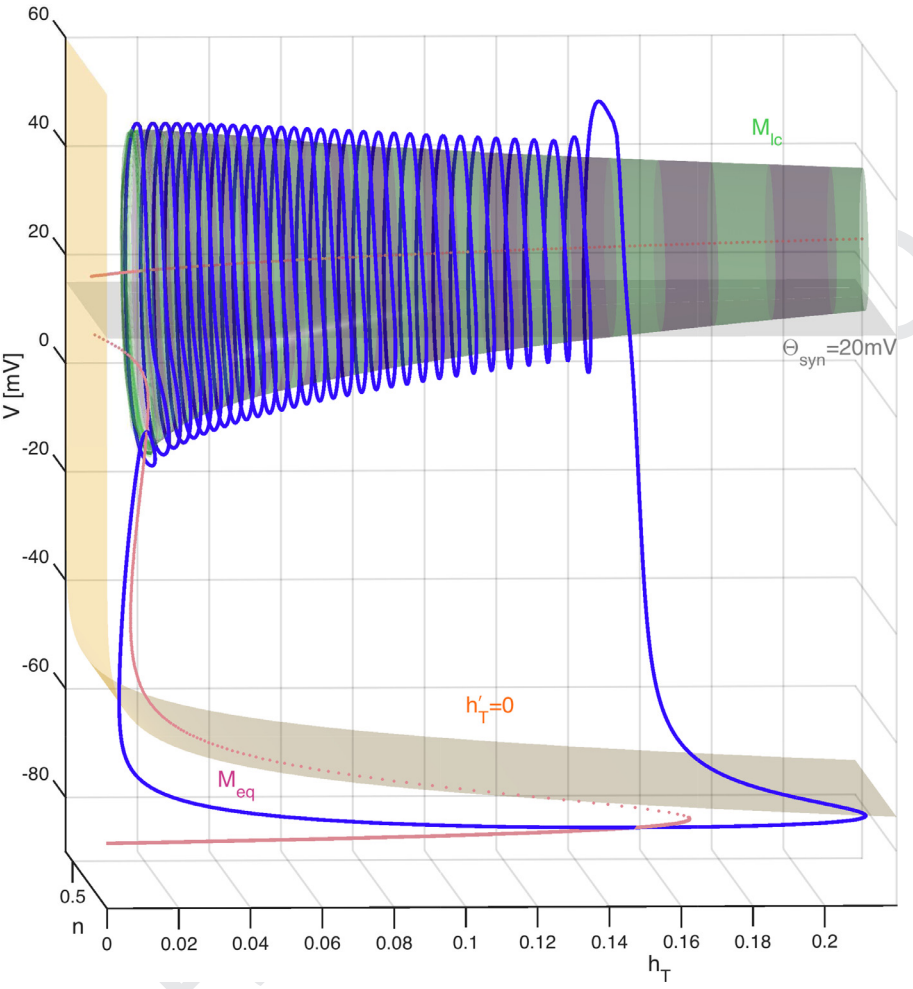

Fig. 1. Bursting orbit (in blue color) recursively switching between two slow-motion critical manifolds: (cylinder-shaped) tonic spiking M_{lc}, and quiescent M_{eq} (orange curve), projected onto the fast (V, n) and slow h_T variables of the neuron model at $I_{ext} = 0$; two other shown surfaces represent the synaptic threshold $\Theta_{syn} = 20$ mV and the slow nullcline $h'_T = 0$, above/below which slow low-threshold Ca^{2+}-current I_T increases/decreases, respectively. The intersection point of $h'_T = 0$ and M_{eq} is an unstable equilibrium state (on the dashed segment) that becomes stable through a super-critical Andronov–Hopf bifurcation after being shifted below the fold at −80 mV onto the hyperpolarized (solid) section of M_{eq}, after the neuron becomes constantly hyperpolarized by the external current I_{ext}, or temporarily by an inhibitory drive from a pre-synaptic neuron. (For interpretation of the references to color in this figure legend, the reader is referred to the web version of this article.)

The low-threshold activated calcium current I_T, modeled by Eq. (10) and regulated by the maximal conductance g_{Ca}, causes the PIR mechanism in the neurons (1), as illustrated in Fig. 2. Here, a rebound burst is triggered by the injection of a hyper-polarizing pulse of the external current $I_{ext}^{(i)}$ (bottom panel in Fig. 2). If the impact of I_T current is strong enough (the impact is stronger for larger values of g_{Ca}), the neuron generates a train of several spikes, after recovering from the hyperpolarized quiescent state (top panel in Fig. 2).

We would like to clarify that even though the system (1) under consideration was specifically aimed at modeling of the voltage dynamics of thalamocortical cells in the original paper [22], our study is not meant to refer to a particular part of brain or nervous system. As such, it is applicable to a broad class of neuronal models of the Hodgkin–Huxley type and an array of PIR based phenomenological systems as a whole. We treat the conductance-based model (1) with certain electrophysiological properties as a generic system, which has turned to possess certain dynamical and bifurcation properties, first of all the PIR mechanism, shared across a large variety of similar systems of diverse biological origins [31]. The features of this single compartment model (1) are based on its two functional components: (i) the first component represents the classical Hodgkin–Huxley-type mechanism for fast spike generation typically due to relaxation oscillations; (ii) the second one is in charge of the calcium-based mechanism for post-inhibitory rebound. Our goal is to understand the "synergetic" interaction of both components: the significance of reciprocal influence of the post-inhibitory rebounds on the fast spiking oscillatory dynamics, and vice verse, in the system of two coupled neurons.

Please cite this article as: R. Nagornov et al., Mixed-mode synchronization between two inhibitory neurons with post-inhibitory rebound, Commun Nonlinear Sci Numer Simulat (2015), http://dx.doi.org/10.1016/j.cnsns.2015.11.024

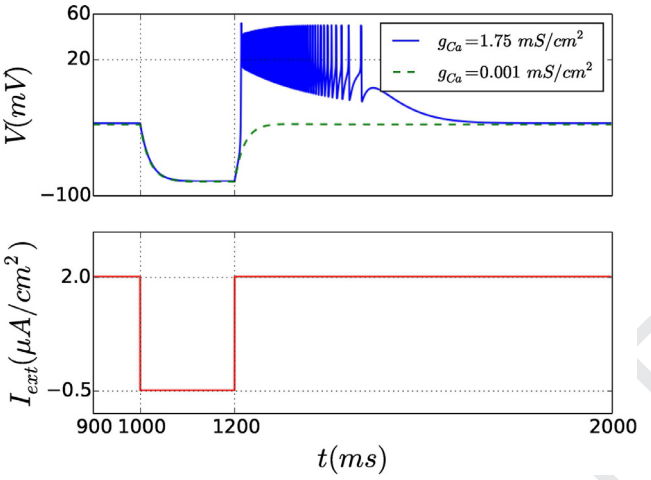

Fig. 2. Abrupt release of a hyperpolarized pulse of the external current I_{ext} (bottom panel) triggers a post-inhibitory rebound of bursting in the quiescent neuron (top panel). The parameter g_{Ca} stated in the legend denotes maximal conductance of the current I_T. When the parameter g_{Ca} is relatively small, the effect of the I_T current is negligible, what causes absence of PIR in the dynamics of the neuron (dashed green curve in the top panel). (For interpretation of the references to color in this figure legend, the reader is referred to the web version of this article.)

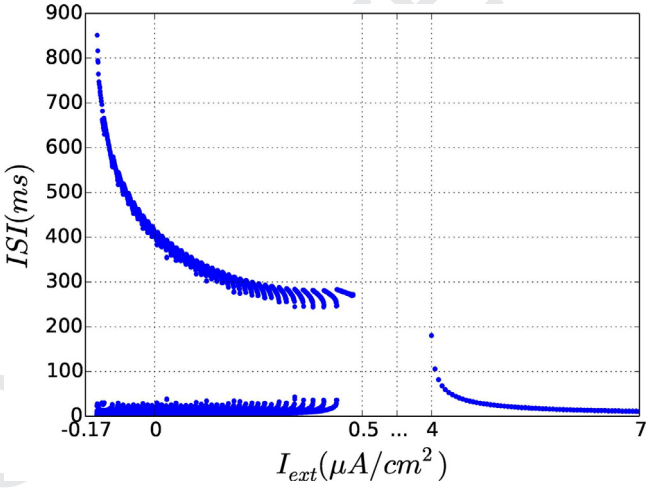

Fig. 3. Bifurcation diagram for an isolated neuron ($g_{Ca} = 1.75\,\mathrm{mS/cm^2}$): plotting inter-spike intervals (ISI) against the external current I_{ext} (this horizontal axis is broken in the middle to highlight the ranges of nontrivial behaviors) reveals windows of bursting ($-0.14\,\mu\mathrm{A/cm^2} \lesssim I_{ext} \lesssim 0.5\,\mu\mathrm{A/cm^2}$), quiescence ($0.5\,\mu\mathrm{A/cm^2} \lesssim I_{ext} \lesssim 4\,\mu\mathrm{A/cm^2}$), and tonic spiking ($I_{ext} \gtrsim 4\,\mu\mathrm{A/cm^2}$) activity in the neuron. The low ISI branch corresponds to short time intervals between fast spikes, and the top branch represents long interburst intervals between consecutive spike trains.

3. Dynamics of an isolated neuron

Let us first consider the dynamics of an isolated neuron at $I_{syn} = 0$ in Eq. (1). The external current I_{ext} is considered to be the pivotal bifurcation parameter that allows one to examine and plausibly model various neuronal activities and transitions between them in both computational and biological experiments. We employ the notion of inter-spike intervals (ISIs) quantifying distances between adjacent spikes generated by the neurons, as the feasible measurement characterizing the types of neuronal activity. Fig. 3 illustrates how the ISIs can change with variations of I_{ext}.

First we describe the neuron dynamics at large I_{ext} values. For $I_{ext} > 4\,\mu\mathrm{A/cm^2}$, the neuron produces tonic spiking activity (corresponding to a stable periodic orbit in the phase space of the model (1)). Here, the value of ISI (which is the period of the stable orbit) is inversely proportional to the I_{ext}-value. The period decreases with increase of I_{ext}, and vice versa. As one can see from Fig. 3, near a critical value $I_{ext} \approx 4\,\mu\mathrm{A/cm^2}$, the ISI shows an "unbounded" growth, which is an indication of a bifurcation of the stable periodic orbit with an arbitrarily long period. Detailed examinations indicate the occurrence of a homoclinic saddle-node bifurcation [14] underlying the transition from the tonic spiking activity to the hyperpolarized quiescence, represented by a stable equilibrium state at low values of the membrane potential V. This stable equilibrium state (a node with real and negative characteristic exponents) persists within the parameter window $0.8\,\mu\mathrm{A/cm^2} \lesssim I_{ext} \lesssim 4\,\mu\mathrm{A/cm^2}$, where the neuron remains ready for PIRs. Small perturbations of the quiescent state of the neuron have no pronounced effects. Relatively strong perturbations

Please cite this article as: R. Nagornov et al., Mixed-mode synchronization between two inhibitory neurons with post-inhibitory rebound, Commun Nonlinear Sci Numer Simulat (2015), http://dx.doi.org/10.1016/j.cnsns.2015.11.024

can trigger a spike, after which the neuron comes back to the over-damped quiescence state. With a decrease of I_{ext} from the threshold $I_{ext} \approx 4\,\mu A/cm^2$, the steady state becomes a focus. The stable focus loses its stability through a supercritical Andronov-Hopf bifurcation at $I_{ext} \approx 0.8\,\mu A/cm^2$ (see the explanation below). These oscillations are not seen in Fig. 3 because they are under the threshold of spike generation. The amplitude of the oscillations increases rapidly as I_{ext} is further decreased. At $I_{ext} \approx 0.5\,\mu A/cm^2$ the shape of the periodic orbit in the phase space changes via the addition of new "turns" around the tonic spiking manifold through the mechanism of period-adding [32,33]. Such a stable periodic orbit is associated with a robust bursting activity, and the number of its turns is exactly the number of the spikes within a burst (see Fig. 1). Bursting that includes two time scales can be recognized in Fig. 3 through two characteristic branches: the bottom branch corresponds to small ISI values due to fast spiking, while the top branch is due to long inter-burst intervals. More details on geometry of bursting can be found in [15,30]. Decreasing the external current I_{ext} makes the bursting neuron more depolarized and increases the number of spikes per burst. Having reached some maximal value of spikes per burst at $I_{ext} \approx -0.136\,\mu A/cm^2$, a further decrease of I_{ext} can cause the neuron to generate bursts with considerably fewer spikes. The value $I_{ext} \approx -0.14\,\mu A/cm^2$ corresponds to the occurrence of another saddle-node bifurcation of equilibria since the time interval between two consecutive bursts becomes arbitrarily large. For $I_{ext} < -0.14\,\mu A/cm^2$ the neuron remains quiescent and excitable.

The examination of bifurcations has been repeated for several values of the maximal conductance g_{Ca}, regulating the low-threshold Ca^{2+} current responsible for PIR in the neuron. We have found that this current bears an insignificant affect on the intrinsic dynamics of the individual neurons, mainly because the membrane potential does not decrease below the threshold value to activate the current. As we will see below, this is not the case for coupled neurons, where the parameter g_{Ca} has a pronounced effect on the collective dynamics.

4. Synchronization of two bursting neurons

In this section and Sections 5–7, we explore a repertoire of rhythmic bursting outcomes generated by a HCO constituted by two neurons coupled reciprocally by fast, non-delayed inhibitory synapses. The current section deals with the dynamics of coupled endogenously bursting neurons. Sections 5 and 6 will focus on intrinsically spiking and quiescent neurons, respectively, that become coupling-induced bursters due to the PIR mechanism. Next, in Section 7 we will consider the mixed-mode case of coupled neurons with different types of intrinsic activity.

It has recently become known that endogenous bursters, when weakly coupled, can produce a range of synchronous rhythmic outcomes with various fixed phase-lags, due to spike interactions within overlapping bursts, see [6,34] and the references therein.

First we will examine the cooperative dynamics in the system of two coupled neurons ($N = 2$ in Eqs. (1)) with different $I_{ext}^{(1,2)}$ within the interval $[-0.14\,\mu A/cm^2,\ 0.5\,\mu A/cm^2]$. This range of the current I_{ext} corresponds to the endogenous bursting in both neurons. Due to the difference, $\Delta I_{ext} = I_{ext}^{(1)} - I_{ext}^{(2)}$, the temporal and quantitative characteristics of endogenous bursters such as their period, duty cycles, the spike numbers per burst, are different. The strength of the coupling is quantified by the maximal conductance G, of the inhibitory synaptic current I_{syn}. In what follows, we show that while ΔI_{ext} remains relatively small, increasing the coupling strength shall give rise to an onset of synchrony between the neurons with the same bursting period in a rather straightforward way (Section 4.1). However, for larger ΔI_{ext} values (Section 4.2) also more complex states are observed. All results in this section are obtained for $g_{Ca} = 1.75\,mS/cm^2$.

4.1. Nearly identical bursters

While $|\Delta I_{ext}| \lesssim 0.05\,\mu A/cm^2$, synchronous bursting can already occur at a relatively weak coupling: the burst periods of both neurons become equal. This observation is supported by Fig. 4, which depicts the dependence of the established (after relatively long transient) phase lag $\Delta\varphi$ on the coupling strength G for several values of the conductance g_{Ca}. Here, $\Delta\varphi$ is introduced as the phase difference:

$$\Delta\varphi = |\varphi_1 - \varphi_2|, \tag{4}$$

where $\varphi_{1,2}$ denote the phases of both endogenous bursters that are defined as follows:

$$\varphi_i = 2\pi \frac{t - T_i^{(k)}}{T_i^{(k+1)} - T_i^{(k)}}, \quad t \in [T_i^{(k)}, T_i^{(k+1)}]. \tag{5}$$

Here, $T_i^{(k)}$ is the initiation moment of the kth burst in the voltage trace $V_i(t)$ $(i = 1, 2)$, and k is greater than some N to skip transients, after which the dynamics settles down onto some fixed phase lag $\Delta\varphi^*$. As one can see from Fig. 4, such a phase locking occurs at about the same coupling constant value (identified by a vertical dashed line in the Fig. 4) for different values of g_{Ca}. Near the threshold of the phase locking, the stationary value of $\Delta\varphi$ is close to $3\pi/2$ (or, equivalently, to $-\pi/2$); here the neurons produce out-of-phase bursts. However, with an increase of the inhibitory coupling over a critical value, the phase lag tends eventually to π, which indicates the occurrence of proper anti-phase bursting in the HCO. Note that the post-inhibitory rebounds in the neurons under consideration are due to the slowest, low-threshold Ca^{2+}-current I_T, whose magnitude is controlled by the maximal conductance g_{Ca}. It is worth noticing that PIRs occur more reliably with increasing g_{Ca}. One can see from Fig. 4 that an increase of g_{Ca} (promoting stronger post-inhibitory rebound activity) may lead to the onset of symmetric antiphase bursting

UNCORRECTED PROOF

Please cite this article as: R. Nagornov et al., Mixed-mode synchronization between two inhibitory neurons with post-inhibitory rebound, Commun Nonlinear Sci Numer Simulat (2015), http://dx.doi.org/10.1016/j.cnsns.2015.11.024

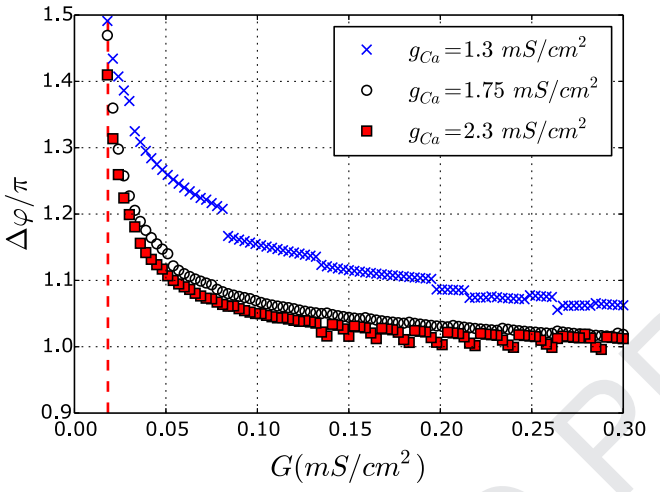

Fig. 4. Stationary value of the phase lag $\Delta\varphi$ (Eq. (4)), plotted vs. the coupling strength G for different values of the maximal conductance g_{Ca} (larger g_{Ca} values promote stronger PIRs in the neurons); here $I_{ext}^{(1)} = 0.2\,\mu A/cm^2$ and $I_{ext}^{(2)} = 0.15\,\mu A/cm^2$.

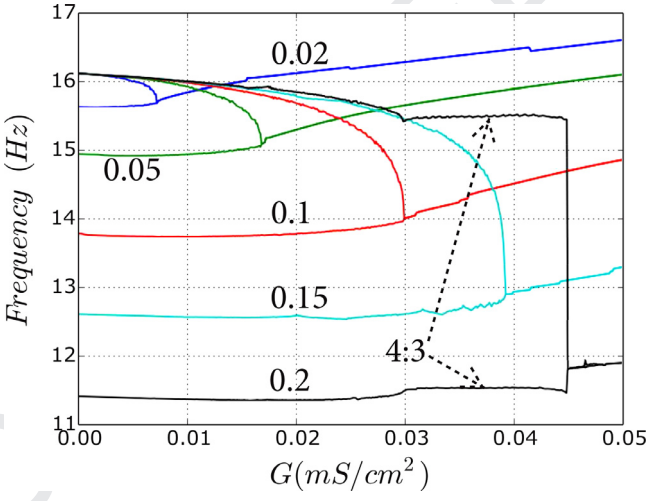

Fig. 5. Bifurcation diagram for antiphase synchronization regimes: averaged frequency of bursting is plotted against the coupling strength for several increasing ΔI_{ext} values. Double overlapping branches are the indication of bursting dichotomy with two slow different frequencies in the two coupled neurons. Note a large plateau of the pronounced 4:3 frequency locking (indicated by dashed arrows) at $\Delta I_{ext} = 0.2\,\mu A/cm^2$, collapsing into anti-phase synchrony locked at an 1:1 ratio at higher G values.

even at small values of the coupling strength. This is an explicit manifestation of the contribution of the slow low-threshold Ca^{2+}-current in fostering the anti-phase synchronization between the bursting neurons in the HCO.

While the in-phase bursting appears to be atypical for neurons with fast inhibitory coupling like in our case, the coexistence of anti-phase and in-phase regimes has been reported elsewhere [4,6]. However, the in-phase synchrony can prevail whenever both HCO neurons are driven externally by another inhibiting burster or a HCO [23,35].

4.2. Bursters that far from identical

Increasing ΔI_{ext} in the coupled oscillators leads to an array of pronounced synchronization effects. Fig. 5 represents the slow (bursting) frequencies plotted against the coupling strength G, for several ΔI_{ext} values. This figure depicts multiple branches of the synchronization locking frequencies at low G-values. This indicates that the coupled neurons generate bursting activities at different frequencies, until the coupling is increased over a threshold value at which both branches merge. This threshold value becomes higher with increasing of ΔI_{ext}, as the individual neurons become more and more distinct. We can see from this figure that for the largest case $\Delta I_{ext} = 0.2\,\mu A/cm^2$, the HCO neurons become locked at the 4:3 frequency ratio (see the plateau, indicated by dashed arrows in Fig. 5), prior to the occurrence of the ultimate 1:1 frequency locking at higher coupling values. It is worth mentioning that complex phase-locking regimes (similar to the case of 4:3 locking) are typical for oscillatory systems with relatively large frequency mismatches, and have been identified as high-order locking regimes in various applications [1].

Please cite this article as: R. Nagornov et al., Mixed-mode synchronization between two inhibitory neurons with post-inhibitory rebound, Commun Nonlinear Sci Numer Simulat (2015), http://dx.doi.org/10.1016/j.cnsns.2015.11.024

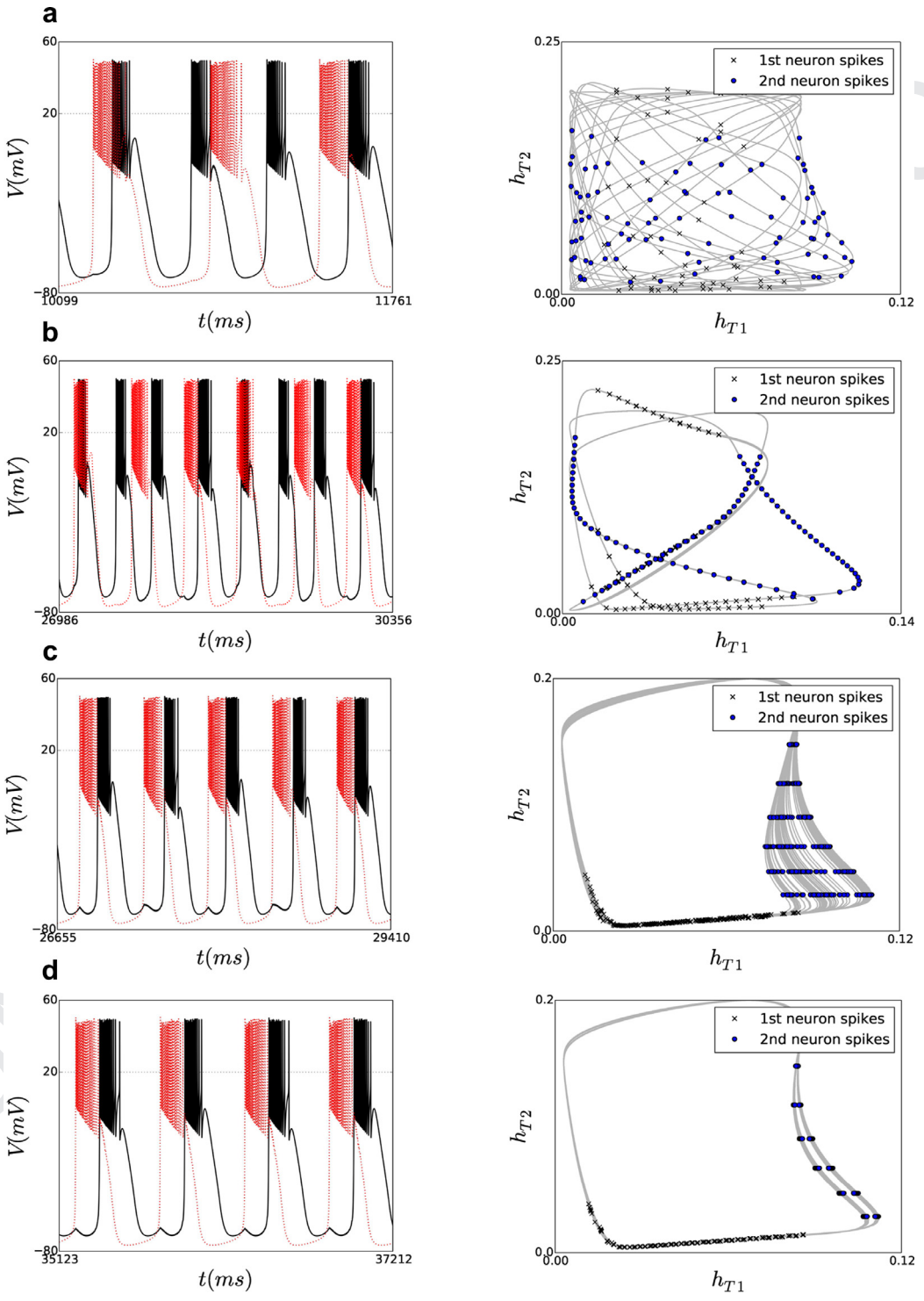

Fig. 6. Left column shows progressions of phase locked voltage traces of two coupled neurons at $\Delta I_{\text{ext}} = 0.2\,\mu\text{A/cm}^2$, $I_{\text{ext}}^{(1)} = 0.2\,\mu\text{A/cm}^2$ for $G = 0.02\,\text{mS/cm}^2$ (a); $0.0445\,\text{mS/cm}^2$ (b); $0.464\,\text{mS/cm}^2$ (c); $0.048\,\text{mS/cm}^2$ (d). Right panels demonstrate the Lissajous curves drawn by slow variables $h_T^{(1)}$ and $h_T^{(2)}$, which correspond to (a) quasi-periodic dynamics at $G = 0.02$; (b) a 4:3-frequency locking regime at $G = 0.0445\,\text{mS/cm}^2$; (c) an 1:1 chaotic locking at $G = 0.464\,\text{mS/cm}^2$; (d) an 1:1 periodic locking at $G = 0.048\,\text{mS/cm}^2$. Circles and squares mark spike events in bursting.

Please cite this article as: R. Nagornov et al., Mixed-mode synchronization between two inhibitory neurons with post-inhibitory rebound, Commun Nonlinear Sci Numer Simulat (2015), http://dx.doi.org/10.1016/j.cnsns.2015.11.024

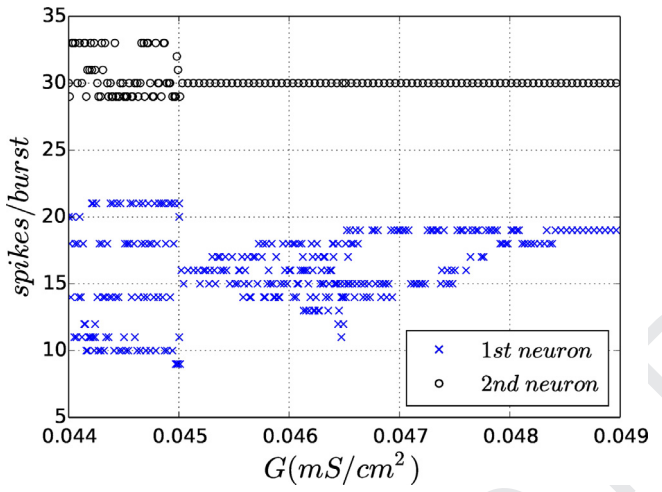

Fig. 7. Bifurcation diagram showing spike number per burst generated by the neurons plotted against the coupling constant G; other parameters are same as in Fig. 6. Value $G \approx 0.045\,\mathrm{mS/cm^2}$ is a threshold towards the 1:1-frequency locking; $G \approx 0.0464\,\mathrm{mS/cm^2}$ corresponds to phase slipping in the chaotic 1:1 locking state of alternating bursting.

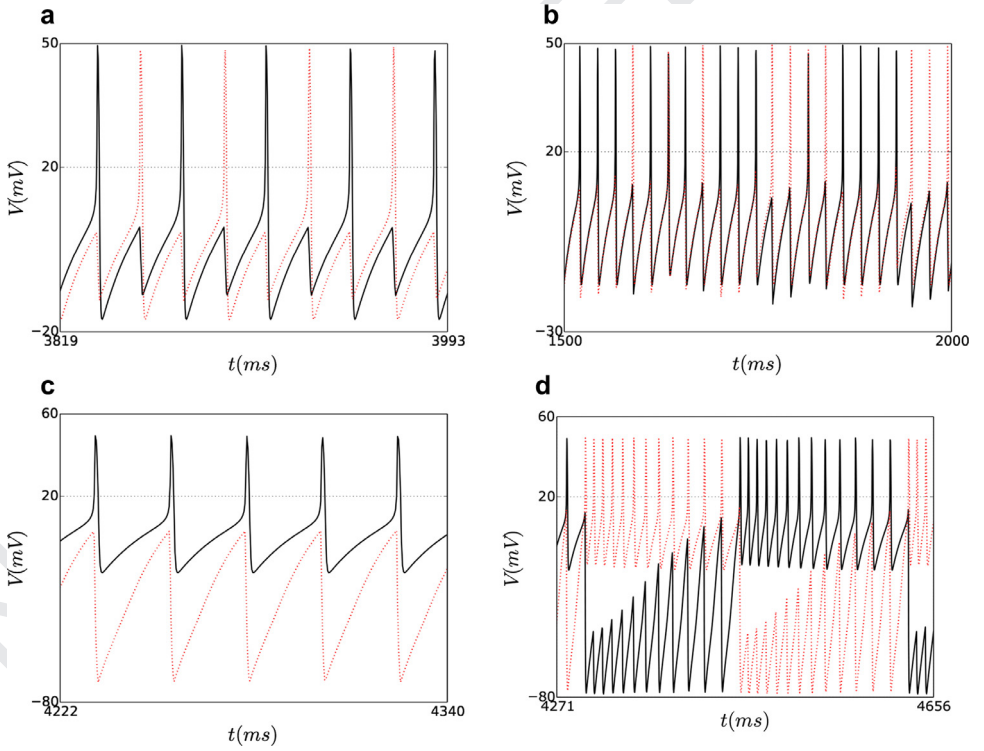

Fig. 8. Voltage oscillatory activity generated by the HCO at $g_{Ca} = 1\,\mathrm{mS/cm^2}$ and $I_{ext}^{(1)} = 5$, and $\Delta I_{ext} = 0.02\,\mu\mathrm{A/cm^2}$: (a) antiphase spiking at $G = 0.2\,\mathrm{mS/cm^2}$; (b) chaotic spiking activity at $G = 0.37\,\mathrm{mS/cm^2}$; (c) forced sub-threshold oscillations (red) in neuron 2 due to fast spiking (black) in neuron 1 at $G = 2\,\mathrm{mS/cm^2}$, (d) coupling-induced bursting at $G = 4\,\mathrm{mS/cm^2}$. (For interpretation of the references to color in this figure legend, the reader is referred to the web version of this article.)

These types of phase synchronizations are characterized by commensurable periods of coupled oscillators such as $3T_1 = 4T_2$. As one can see in Fig. 5, for all values of ΔI there always exists a threshold value of the coupling constant G, beyond which the anti-phase 1:1 synchronization takes place. Expectedly, the threshold increases with increase of ΔI. The latter properties remain true even for larger values of mismatch ΔI, so far both neurons are in the range of intrinsic bursting.

Fig. 6 illustrates transitions to synchrony between the neurons in the HCO for the largest case $\Delta I_{ext} = 0.2\,\mu\mathrm{A/cm^2}$. The left panels depict the established anti-phase bursting in voltage traces produced by the HCO at various values of the coupling strength G, below and above the 1:1 synchronization threshold. The right panels represent the so-called Lissajous curves, which are parametrically traced down by the slow variables $h_T^{(1)}$ and $h_T^{(2)}$ of both neurons. These curves help one to interpret the corresponding

Please cite this article as: R. Nagornov et al., Mixed-mode synchronization between two inhibitory neurons with post-inhibitory rebound, Commun Nonlinear Sci Numer Simulat (2015), http://dx.doi.org/10.1016/j.cnsns.2015.11.024

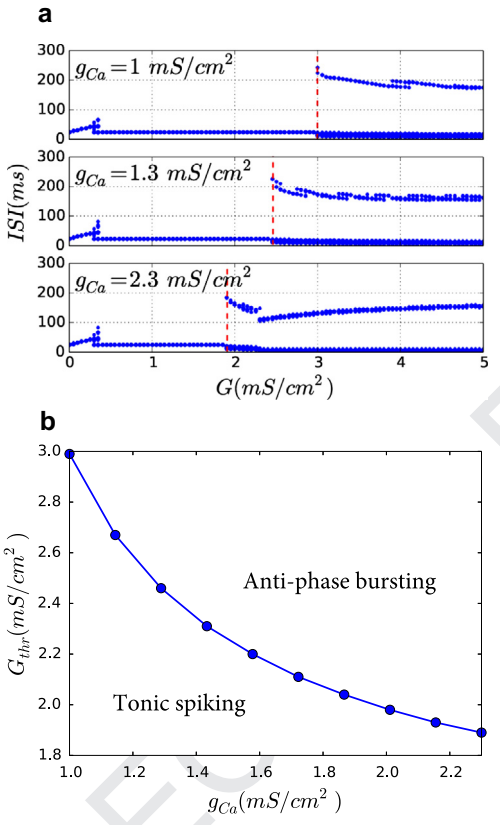

Fig. 9. (a) Diagram representing inter-spike intervals plotted against the coupling constant G for three increasing values of g_{Ca} indicated by labels on the corresponding panels. Due to similarity, the diagram is presented for the first neuron. Vertical dashed lines indicate the transition thresholds to emergent anti-phase bursting. (b) Critical value of the coupling constant G plotted against the maximal conductance of I_T current. For $G < G_{thr}$ the network stably inhibits antiphase spiking (one ISI value corresponds to one G value); for $G > G_{thr}$ the system obtains stable antiphase bursting regime (few ISI values correspond to one G value). Parameters for both panels are $I_{ext\,1} = 5\,\mu A/cm^2$ and $\Delta I_{ext} = 0.02\,\mu A/cm^2$ (corresponding to tonic spiking neurons in isolation).

types of frequency locking, including quasi-periodic dynamics. Dots on these curves in the right panels mark timing of individual spikes in bursts.

It is worth noticing that at larger values of ΔI_{ext}, the phase difference $\Delta\varphi$ (Eq. (4)) tends to converge to $\pi/2$, rather than to π, as the coupling strength G is increased. With a $\pi/2$ phase shift, active phases of bursting in the neurons partially overlap (one expects strong overlap for a zero or small phase shift and no overlap for anti-phase oscillations, i.e. for a phase shift close to π), showing the emergence of the complex dynamics caused by spike interactions. To understand this dynamics, we evaluated the distribution of numbers of spikes per burst for several coupling strengths. Our findings are presented in Fig. 7. The analysis of the bursting frequency (not shown, similar to Fig. 5) reveals that the transition to the 1:1 locking occurs at $G \approx 0.045\,\mathrm{mS/cm^2}$. Moreover, our simulations indicate that there is a small window, $\Delta G \approx 1.5 \times 10^{-4}\,\mathrm{mS/cm^2}$, of a hysteresis occurring at the transition. Fig. 7 reveals a peculiar feature of the synchronous state (in the sense of coincidence of the average bursting periods of two neurons), occurring at strong coupling $G \in [0.045\,\mathrm{mS/cm^2}, 0.0485\,\mathrm{mS/cm^2}]$: while the spike number in bursts generated by neuron 2 remains nearly the same, the number of spikes in bursts by neuron 1 shows a large dispersion, before it becomes a constant at a stronger coupling.

From the two bottom insets in Fig. 6(c) and (d) one can observe that depending on the coupling strength, the 1:1 locking can exhibit chaotic and periodic modulations via the slow gating variables of the neurons. Chaotic modulation is depicted in Fig. 6(c). Here one can clearly see spreading of slow variables on the Lissajous curves, typical for low-dimensional strange attractors (chaoticity here was confirmed by observation of irregular variations of the number of spikes in bursts: autocorrelation function of this observable decays for the chaotic case and returns to one for the quasiperiodic dynamics). The number of spikes per burst in the second neuron varies significantly for chaotic modulation. One can see this in Fig. 7 at the corresponding value of coupling: at $G = 0.464\,\mathrm{mS/cm^2}$ the first neuron shows from 13 to 18 spikes per burst. On the other hand, the alternating bursting in the HCO remains locked at an 1:1-ratio of the bursting frequencies. This is an explicit manifestation of the phenomenon of chaotic phase synchronization in slow-fast dynamics [5]. Indeed, chaotic phase synchronization is a regime in coupled chaotic oscillators, which are synchronized in mean periods only (the phases are locked), while amplitudes remain chaotic and non-synchronized. In the context of our Hogkin–Huxley-type neurons, the slow dynamics just show such a behavior, while the uncorrelated slow chaotic amplitudes manifest themselves, quite spectacular, in the variations in the number of spikes per burst. Periodic modulation is

Please cite this article as: R. Nagornov et al., Mixed-mode synchronization between two inhibitory neurons with post-inhibitory rebound, Commun Nonlinear Sci Numer Simulat (2015), http://dx.doi.org/10.1016/j.cnsns.2015.11.024

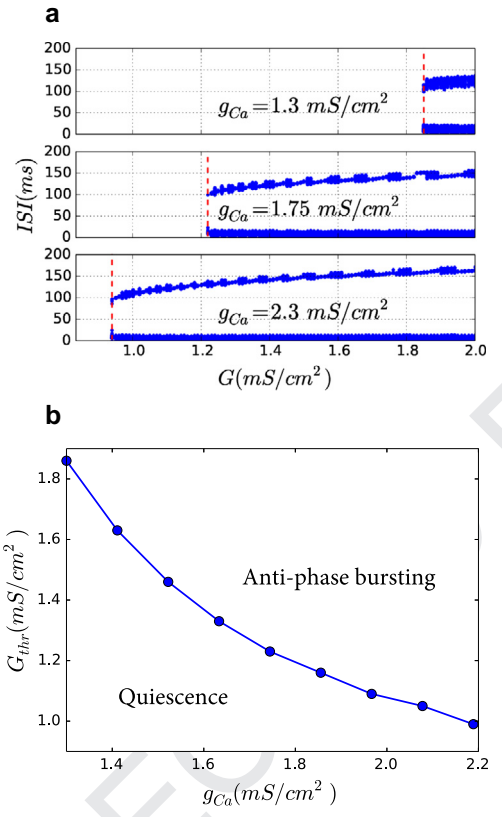

Fig. 10. (a) Diagram of inter-spike intervals in neuron 1 plotted against the coupling constant G for three increasing values of g_{Ca} indicated by labels on the corresponding panels; vertical dashed lines indicates the transition thresholds to emergent anti-phase bursting. (b) Critical value of the coupling constant G plotted against the maximal conductance of I_T current. For $G > G_{thr}$, the system stably exhibits anti-phase bursting regime. Parameters for both panels are $I_{\text{ext}}^{(1)} = 2\,\mu\text{A/cm}^2$ and $\Delta I_{\text{ext}} = 0.02\,\mu\text{A/cm}^2$ (corresponding to both hyperpolarized quiescent neurons in isolation).

depicted at the bottom row of Fig. 6(d). Here one can see that the Lissajous curve splits in two lines. Correspondingly, at this value of coupling ($G = 0.048\,\text{mS/cm}^2$) the first neuron, according to Fig. 7, shows alternating bursts with 18 and 19 spikes.

5. Antiphase bursting out of spiking neurons

In this section we study the emergence of alternating bursting in a HCO made of two coupled neurons that are tonically spiking being in isolation at $I_{\text{ext}}^{(1)} = 5\,\mu\text{A/cm}^2$, with relatively small $\Delta I_{\text{ext}} = 0.02\,\mu\text{A/cm}^2$. Our goal is to reveal how increasing of the inhibitory coupling strength transforms such tonic spikers into coupling-induced bursters, as illustrated in Fig. 8.

Weak coupling results in a periodic antiphase tonic spiking in the coupled neurons at $G = 0.2\,\text{mS/cm}^2$ (Fig. 8(a)). With further increase of the coupling strength, the HCO neurons first demonstrate irregular, unreliable spiking around $G = 0.37\,\text{mS/cm}^2$, as shown in Fig. 8b. The mechanism of chaoticity here is similar to that for other slow-fast oscillators featuring canards [3]. In such a system, sensitive irregularity is typically observed whenever its solutions pass nearby the borderline of the slow motion manifold, and hence, depending on tiny perturbations, can produce an extra spike [36–38]. With further increase of the coupling strength, an asymmetric dynamics is observed. In this robust regime, either neuron generates tonic spiking activity, while the other one is forced to produce sub-threshold oscillations of quite a large amplitude, such as ones shown in Figs. 8(b) and (c) at $G = 2\,\text{mS/cm}^2$. A dramatic increase in the inhibitory coupling strength beyond $G \approx 3\,\text{mS/cm}^2$ finally forces the neurons to begin bursting in alternation.

Such a bursting activity is often referred to as a coupling-induced bursting, which is the result of strongly reciprocal interactions of two individually tonic spiking neurons. Fig. 3 provides an explanation, why inhibitory coupling must be strong enough to be able to induce coupling-induced bursting in the given model. There is a wide gap between the values of parameter I_{ext} corresponding to bursting (at the low end) and to tonic spiking (on the high end). Within this gap, the neurons remain hyperpolarized quiescent, and hence the bursting can only occur through PIR mechanisms. A strong flux of inhibitory current is required to originate from the presynaptic, tonic spiking neuron in order to activate the low-threshold I_T current in the postsynaptic neuron. The positive exciting effect of the current I_T can overcome the inhibition and trigger the onset of the post-rebound activity. Then, the neurons swap the roles of the driving and the driven units in the HCO, so that the process keeps repeating. This assertion is further supported by Fig. 9(a), showing inter-spike intervals (ISIs) of the neurons vs. the coupling strength for three values of

Please cite this article as: R. Nagornov et al., Mixed-mode synchronization between two inhibitory neurons with post-inhibitory rebound, Commun Nonlinear Sci Numer Simulat (2015), http://dx.doi.org/10.1016/j.cnsns.2015.11.024

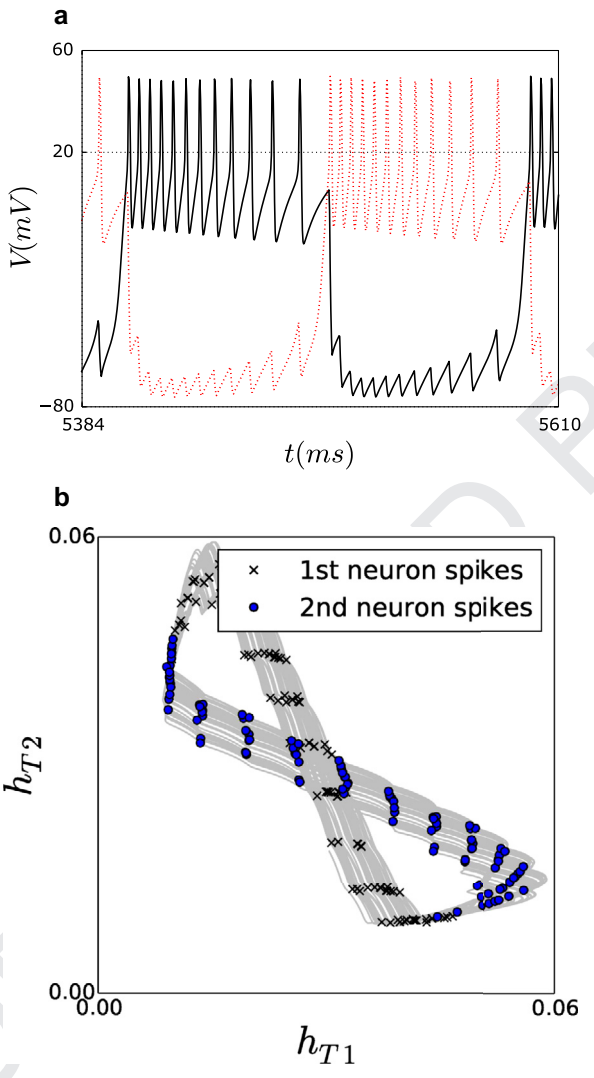

Fig. 11. (a) Antiphase coupling-induced bursting through the PIR mechanism is filled out densely by alternating voltage traces without quiescent gaps unlike the case of coupled endogenous bursters through the release mechanism. (b) Lissajous curve of a figure-eight shape traced down by the slow gating variables of the models at $G = 1.24\,\mathrm{mS/cm^2}$ and $g_{Ca} = 1.75\,\mathrm{mS/cm^2}$; other parameters the same as in Fig. 10. Circles and crosses in panel (b) mark occurrences of spikes.

g_{Ca}. To the left of the vertical dashed line the system is either in the regime of anti-phase tonic spiking (voltage traces are similar to Fig. 8(a) and (b)), or in the regime of tonic spiking of only one neuron, and suppression of another one (Fig. 8(c)). Here one can see, that for all three values of g_{Ca} the system switches to the bursting mode, which is characterized by two branches of inter-spike intervals (on the right of the vertical dashed lines in Fig. 9(a)). In all cases the latter regime is anti-phase synchronous bursting depicted in Fig. 8(d). As one can see, the value of g_{Ca} drastically changes the threshold, at which bursting stably occurs (compare positions of the vertical dashed lines at different panels in Fig. 9(a)). Indeed, Fig. 9(b) summarizes the qualitative role of the slow low-threshold Ca^{2+}-current I_T: an increase of the corresponding rebound parameter g_{Ca} lowers the threshold of coupling-induced bursting, and narrows the parameter interval of hyperpolarized quiescence in the neurons.

We would like to emphasize that in this section we have considered intrinsically spiking neurons. Here anti-phase bursting appears as a result of strong synaptic coupling, which is sufficient to switch the neurons from the spiking mode to the bursting regime. Hence, parameter ΔI and difference in spiking frequencies do not play a crucial role here, and can be relatively large in order to get anti-phase bursting.

6. P.I.R. mechanism for antiphase bursting

In this section we examine the emergence of coupling-induced anti-phase bursting through the PIR mechanism. Here, it is imperative that both neurons remain hyperpolarized quiescent within a parameter window $0.5\,\mu\mathrm{A/cm^2} \lesssim I_{\mathrm{ext}} \lesssim 4\,\mu\mathrm{A/cm^2}$, as seen from Fig. 3. It is also necessary for PIR coupling-induced bursting, that the initial states of the neurons must be different:

Please cite this article as: R. Nagornov et al., Mixed-mode synchronization between two inhibitory neurons with post-inhibitory rebound, Commun Nonlinear Sci Numer Simulat (2015), http://dx.doi.org/10.1016/j.cnsns.2015.11.024

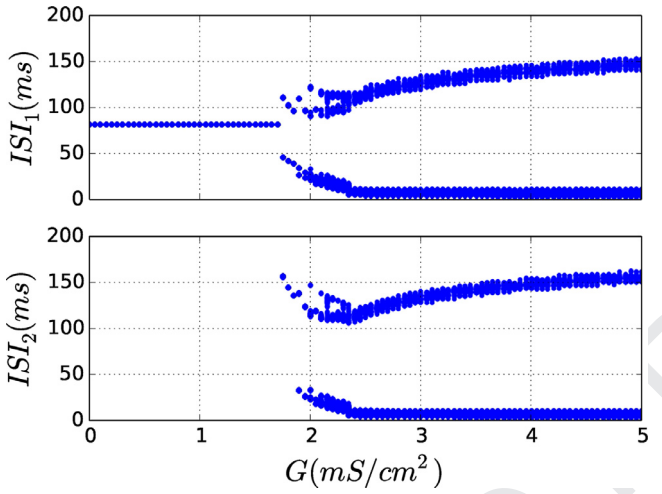

Fig. 12. Bifurcation diagram of ISIs plotted versus the coupling parameter G indicates the threshold, beyond which the system comprised of the tonically spiking neuron 1 and the hyperpolarized quiescent neuron 2 begins to generate anti-phase bursting; $g_{Ca} = 1.75\,\mathrm{mS/cm^2}$.

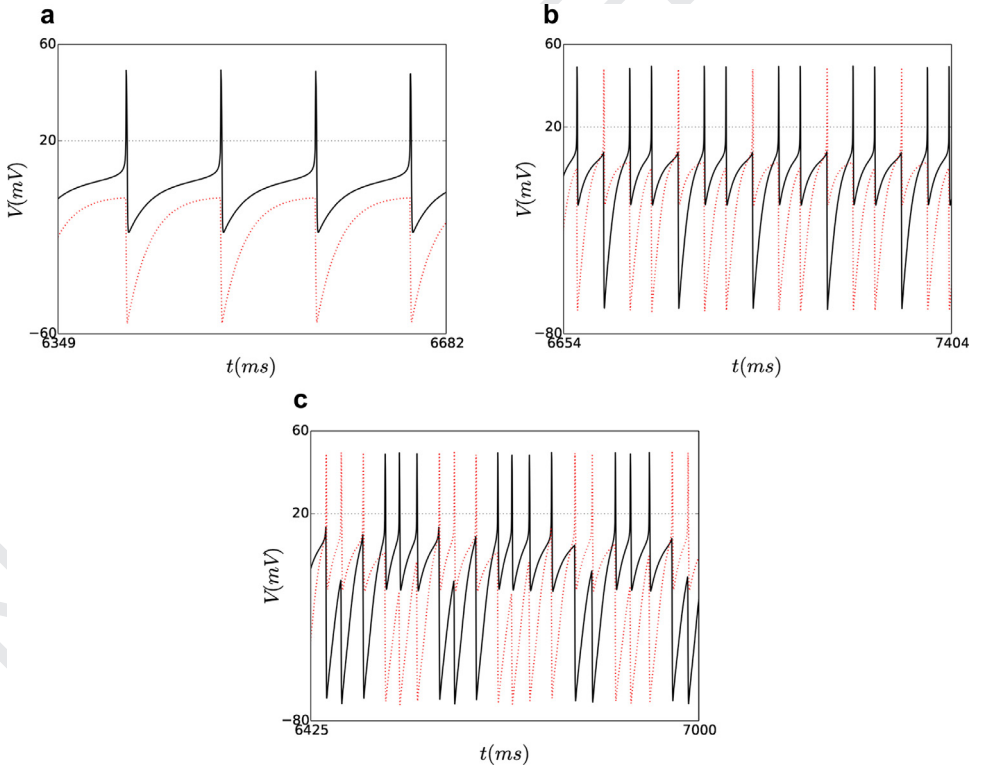

Fig. 13. Voltages patterns generated by the HCO neurons: (a) tonic spiking (black) in neuron 1 and inhibition induced subthreshold oscillations (red) in neuron 2 at $G = 1\,\mathrm{mS/cm^2}$; (b) periodic antiphase spiking with a 2:1 locked ratio at $G = 1.8\,\mathrm{mS/cm^2}$; (c) chaotic antiphase bursting near the threshold at $G = 2\,\mathrm{mS/cm^2}$.

one at tonic spiking and one being hyperpolarized quiescent. An alternative is an application of a negative pulse of the current to trigger a PIR in the targeted neuron. In addition to the above constrains, the coupling strength must exceed a certain threshold, as indicated by the vertical dashed lines in Fig. 10(a).

One can see from this plot, that relatively weak coupling cannot initiate PIR coupling-induced bursting. Rather, some sub-threshold oscillations are generated in the post-synaptic neuron, which extinct as soon as the pre-synaptic neuron ends its active spiking phase, and becomes hyper-polarized quiescent as well. For each set of the parameters, numerical simulations depicted in Fig. 10(a) clearly show that there is a threshold for the coupling strength, beyond which the HCO robustly produces anti-phase bursting. Figure 10(b) also demonstrates that the PIR mechanism of coupling-induced bursting becomes more reliable

Please cite this article as: R. Nagornov et al., Mixed-mode synchronization between two inhibitory neurons with post-inhibitory rebound, Commun Nonlinear Sci Numer Simulat (2015), http://dx.doi.org/10.1016/j.cnsns.2015.11.024

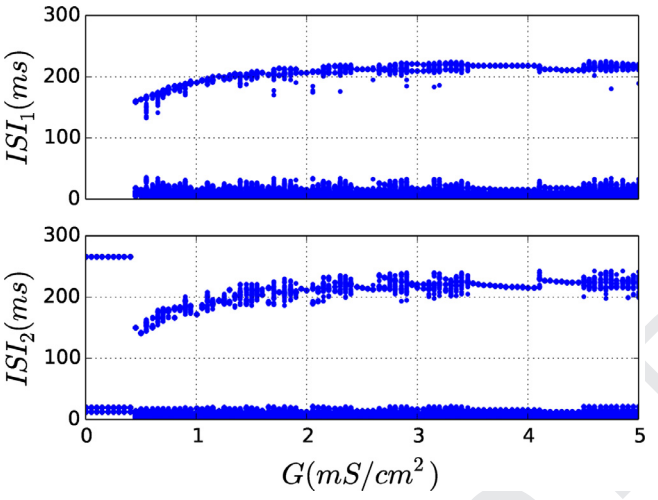

Fig. 14. Bifurcation diagram of ISI plotted against the coupling parameter G indicates the threshold around 0.5 mS/cm^2 beyond which the system made of the bursting neuron 2 and the hyperpolarized quiescent neuron 1 begins to generate anti-phase bursting; here $g_{Ca} = 1.75$ mS/cm^2.

with increasing g_{Ca}, which lowers the threshold value of inhibitory coupling. The PIR bursting is illustrated in Fig. 11(a). Fig. 11(b) reveals a quasi-periodic modulation of the slow gating variables; here the Lissajous curve forms a band of a characteristic figure-eight shape.

7. Coupling of neurons in different regimes

In this section we consider the dynamics of two coupled neurons operating in different modes. Specifically, the neurons are set close to "quiescence-spiking" and "quiescence-bursting" transitions, respectively. As Fig. 3 suggests, we choose the following values of the external driving current: $I_{\text{ext}}^{(1)} = 4.1\,\mu\text{A/cm}^2$ and $I_{\text{ext}}^{(2)} = 3.7\,\mu\text{A/cm}^2$. This means that in isolation neuron 1 produces tonic spiking activity, while neuron 2 is hyperpolarized and ready for the PIR mechanism. Our simulations of two such neurons are summarized in Figs. 12 and 13. We can conclude that while coupling remains weak, neuron 1 tonically spikes (Fig. 13(a)). Above a threshold, $G \approx 1.75$ mS/cm^2, neuron 2 begins spiking as well. Fig. 13(b)) depicts alternating spiking at $G = 1.8$ mS/cm^2 with the locking ratio 2:1, which means that two spikes in neuron 1 are followed by a single spike in neuron 2. The system begins to burst in antiphase, first with irregularly varying numbers of spikes per bursts as G exceeds 2 mS/cm^2, as illustrated in Fig. 13(c). Further increase in the coupling strength above $G = 2.5$ mS/cm^2, regularizes bursting that becomes stable and similar to the pattern shown in Fig. 11.

Figure 14 represents the bifurcation diagram for the endogenous burster – neuron 2 at $I_{\text{ext}}^{(2)} = 0.4\,\mu\text{A/cm}^2$, coupled with neuron 1 remaining hyperpolarized at $I_{\text{ext}}^{(1)} = 1\,\mu\text{A/cm}^2$. Because the quiescent neuron 1 initially remains below the synaptic threshold, anti-phase bursting may only start when the PIR mechanism is induced by the endogenous burster. This explains a qualitative resemblance of the diagram in Fig. 14 to that in Fig. 12, for the HCOs made of tonic-spiking and quiescent neurons.

8. Conclusions

This study is focused on the mechanisms of rhythmogenesis of anti-phase bursting in HCO consisting of two reciprocally inhibitory coupled neurons. Such HCOs are primary building blocks for larger neural networks, including CPGs controlling a plethora of locomotion behaviors in spineless and non-invertebrate animals. There is a growing consensus in the neuroscience community that CPGs of various animals may share same universal principles of their functioning.

In this paper, to study the HCO dynamics, we have used the biophysically plausible Hodgkin-Huxley-type model. Its main feature is the post-inhibitory rebound dynamics: a quiescent neuron is able to produce a single or series of spikes after it has been quickly released from inhibition by another pre-synaptic neuron, or by a hyperpolarized pulse of external current. The PIR mechanism allows a pair of naturally quiescent neurons to stably generate anti-phase oscillations, initiated by virtue of external perturbation(s).

In this study, we have investigated properties of anti-phase bursting through PIR mechanisms, by considering neurophysiologically feasible models. Unlike reduced PIR models, such as 2D slow-fast relation oscillators, the given 7D model with multiple time scales can exhibit a range of complex oscillatory activities. This makes its analytical treatment hardly possible to perform. Instead, we have performed a series of numerical simulations aimed at a quantitative assessment and a qualitative interpretation of the observed dynamical regimes from the viewpoint of general theory of nonlinear dynamical systems. We expect that similar regimes can be observed in other models of Hodgkin-Huxley type, apart from some quantitative differences.

Please cite this article as: R. Nagornov et al., Mixed-mode synchronization between two inhibitory neurons with post-inhibitory rebound, Commun Nonlinear Sci Numer Simulat (2015), http://dx.doi.org/10.1016/j.cnsns.2015.11.024

UNCORRECTED PROOF

We have considered several configurations of HCOs including coupled endogenous bursters. We have also discussed HCOs comprised of tonic spiking and quiescent neurons, that become coupling-induced bursters when coupled by fast inhibitory synapses. In our examination of synchronization properties of bursting, we have found that, in all considered cases, the system of two coupled neurons can reliable achieve synchrony in anti-phase bursting. We have described some particular configurations leading to incomplete synchronization, where the neurons become partially synchronized through slow-varying currents. Meanwhile, cross-correlations in their fast voltage dynamics are not always obvious. This fast voltage dynamics may give rise to the emergence of really complex states, including chaos in the neural ensemble.

We have found that while enhancing the PIR mechanism does not always lead to drastic changes in the dynamics of the individual neurons, it can cause significant modification of the dynamics under coupling. Specifically, we have detected that the windows of anti-phase bursting rhythms can be extended in the parameter space of the system, when increase of the PIR mechanisms in individual neurons becomes more prominent. This suggests that PIR is a key component for robust and stable anti-phase bursting in HCOs. In the future, we plan to examine specific networks constituted by several coupled HCOs, which have been identified in swim CPGs of specific sea mollusks.

Acknowledgments

The research is supported by the grant (the agreement of August 27, 2013 N 02.B.49.21.0003 between The Ministry of Education and Science of the Russian Federation and Lobachevsky State University of Nizhni Novgorod, Sections 2-4) and by the Russian Science Foundation (Project No. 14-12-00811, Sections 5-7). A.P. thanks A. Politi for interesting discussions and acknowledges the G. Galilei Institute for Theoretical Physics (Italy) for the hospitality and the INFN for partial support during the completion of this work. M.K. thanks Alexander von Humboldt foundation for support. A.S. also acknowledges the support from NSF grants DMS-1009591 and IOS-1455527, RFFI 11-01-00001, and RSF grant 14-41-00044 at the Lobachevsky University of Nizhny Novgorod. We thank A. Kelley for helpful suggestions.

Appendix. Conductance based model

The model in this study is adopted from Ref. [22]. The dynamics of the membrane potential, V is governed by the following equation:

$$C_m V' = I_{\text{ext}} - I_T - I_{leak} - I_{Na} - I_K - I_{syn}, \tag{6}$$

here, $C_m = 1\ \mu F/cm^2$ is the specific membrane capacity, I_{ext} is the external current in μA/cm^2, I_T is the slow low-threshold Ca^{2+}-current, I_{leak} is the leakage current, I_{Na} is the Na^+-current, I_K is the K^+-current and I_{syn} is the synaptic current from other neurons.

The leak current I_{leak} is given by

$$I_{leak} = g_{Na}(V - E_{leak}), \tag{7}$$

with $E_{leak} = -78\ mV$ being the reversal potential for leak current, and maximal conductance $g_L = 0.05$ mS/cm^2. Dynamics of the fast Na^+-current $I_{Na} = g_{Na} m^3 h (V - E_{Na})$ is described by the following equations:

$$\begin{aligned} m' &= \frac{0.32(13-V)}{e^{0.25(13-V)}-1}(1-m) - \frac{0.28(V-40)}{e^{0.2(V-40)}-1}m, \\ h' &= 0.128 \cdot e^{\frac{17-V}{18}}(1-h) - \frac{4}{e^{-0.2(V-40)}+1}h, \end{aligned} \tag{8}$$

where $g_{Na} = 100$ mS/cm^2 is the maximal conductance of Na^+-current, $E_{Na} = 50$ mV is the reversal potential for Na^+-current, m and h are the gating variables describing activation and inactivation of the current. Dynamics of the fast K^+-current I_K is described by

$$\begin{aligned} I_K &= g_K n^4 (V - E_K), \\ n' &= \frac{0.032(15-V)}{e^{0.2(15-V)}-1}(1-n) - 0.5 e^{\frac{(10-V)}{40}} n, \end{aligned} \tag{9}$$

with n being the gating activation variable; here $E_K = -95$ mV and $g_K = 10$ mS/cm^2. Dynamics of the slow low-threshold Ca^{2+}-current I_T is modeled as follows:

$$I_T = g_{Ca} m_T^2 h_T (V - E_{Ca}), \tag{10}$$

with $g_{Ca} = 1.75$ mS/cm^2.

The equilibrium potential E_{Ca}, which depends on the intraneuronular concentration of Ca^{2+}, is found from the Nernst equation:

$$E_{Ca} = \bar{k}\frac{R \cdot T}{2F} ln\left(\frac{[Ca]_0}{[Ca]}\right), \tag{11}$$

Please cite this article as: R. Nagornov et al., Mixed-mode synchronization between two inhibitory neurons with post-inhibitory rebound, Commun Nonlinear Sci Numer Simulat (2015), http://dx.doi.org/10.1016/j.cnsns.2015.11.024

UNCORRECTED PROOF

here $R = 8.31441$ J K/mol, $T = 309.15$ K , dimensionless constant $\bar{k} = 1000$ for E_{Ca} is measured in millivolts, the extraneuronular concentration of calcium ions is $[Ca]_0 = 2$ mM.

The gating activation m and the inactivation h are given by

$$m_T' = -\frac{m_T - m_{T\infty}(V)}{\tau_{Tm}(V)}, \quad h_T' = -\frac{h_T - h_{T\infty}(V)}{\tau_{Th}(V)}, \tag{12}$$

with

$$\begin{aligned} m_{T\infty}(V) &= \frac{1}{1+e^{-\frac{V+52}{7.4}}}, \\ \tau_{Tm}(V) &= 0.44 + \frac{0.15}{(e^{\frac{V+27}{10}} + e^{-\frac{V+102}{15}})}, \\ h_{T\infty}(V) &= \frac{1}{1+e^{\frac{V+80}{5}}}, \\ \tau_{Tm}(V) &= 62.7 + \frac{0.27}{(e^{\frac{V+48}{4}} + e^{-\frac{V+407}{50}})}. \end{aligned} \tag{13}$$

These constants were taken at temperature 36 °C and extraneuronular calcium concentration $[\mathrm{Ca}]_0 = 2$ mM.

Dynamics of intraneuronular concentration of calcium ions $[Ca]$ is described via

$$[Ca]' = -\frac{kI_T}{2Fd} - \frac{K_T[Ca]}{[Ca] + K_d}, \tag{14}$$

where the first term is an inflow through thin membrane due to a low-threshold Ca^{2+}-current, and the second term is a contribution of Ca^{2+} ion-pump. Here the parameters are the following: $F = 96,469$ C/mol, $d = 1\,\mu$m, $k = 0.1$, $K_T = 10^{-4}$ mM/m s^{-1} and $K_d = 10^{-4}$ mM.

Synaptic currents are modeled using the fast-threshold modulation paradigm [28]:

$$I_{syn}(V_i, V_j) = G \cdot S(V_j - \theta_{syn}) \cdot (V_i - E_{syn}), \tag{15}$$

where G is the maximal conductance of synaptic current flowing from pre-synaptic jth neuron into the post-synaptic ith neuron. For inhibitory coupling we set $E_{syn} = -80$ mV; the synaptic activity function $S(V)$ is given by

$$S(V) = \frac{1}{1+e^{-100(V-\theta_{syn})}}, \tag{16}$$

with the synaptic threshold $\theta_{syn} = 20$ mV set in a middle of fast spikes.

In numerical simulations of the described model we used the 4th order Runge–Kutta method with time step 0.01.

References

[1] Pikovsky A, Rosenblum M, Kurths J. Synchronization: a universal concept in nonlinear sciences Cambridge nonlinear Science series. Cambridge University Press; 2003.
[2] Shilnikov A, Shilnikov L, Turaev D. On some mathematical topics in classical synchronization: a tutorial. J Bifurc Chaos 2004;14(7):2143–60.
[3] Desroches M, Guckenheimer J, Krauskopf B, Kuehn C, Osinga HM, Wechselberger M. Mixed-mode oscillations with multiple time scales.. SIAM Rev 2012;54(2):211–88.
[4] Jalil S, Belykh I, Shilnikov A. Fast reciprocal inhibition can synchronize bursting neurons. Physical Review E April 2010;81(4, 2).
[5] Omelchenko I, Rosenblum M, Pikovsky A. Synchronization of slow-fast systems. Eur Phys J-Spec Top December 2010;191(1):3–14.
[6] Jalil S, Belykh I, Shilnikov A. Spikes matter for phase-locked bursting in inhibitory neurons. Phys Rev E March 22 2012;85(3, 2).
[7] Wojcik J, Schwabedal J, Clewley R, Shilnikov AL. Key bifurcation of bursting polyrhythms in 3-cell central pattern generators. PLoS ONE 2014;9(4).e92918
[8] Selverston A, editor. Model neural networks and behavior.. Berlin: Springer; 1985.
[9] Marder E, Calabrese RL. Principles of rhythmic motor pattern generation. Physiol Rev 1996;76(3):687–717.
[10] Gillner S, Wallen P. Central pattern generators for locomotion, with special references to vertebrates. Ann Rev Neurosci 1985;8:233–61.
[11] Rabinovich MI, Varona P, Selverston AI, Abarbanel HDI. Dynamical principles in neuroscience. Rev Mod Phys November 2006;78:1213–65.
[12] Shaw KM, Lyttle DN, Gill JP, Cullins MJ, McManus JM, Lu H, et al. The significance of dynamical architecture for adaptive responses to mechanical loads during rhythmic behavior. J Comput Neurosci 2014:1–27.
[13] Schwabedal J, Neiman AB, Shilnikov AL. Robust design of polyrhythmic neural circuits. Phys Rev E August 2014;90:022715.
[14] Shilnikov L, Shilnikov A, Turaev D, Chua L. Methods of qualitative theory in nonlinear dynamics, Parts I and II. World Scientific Publ.; 1998, 2001.
[15] Izhikevich EM. Dynamical systems in neuroscience.. Cambridge, Mass.: MIT Press; 2007.
[16] Hill AAV, Hooser SV, Calabrese RL. Half-center oscillators underlying rhythmic movements. The handbook of brain theory and neural networks. Arbib MA, editor. The MIT Press; 2003.
[17] Wang X-J, Rinzel J. Alternating and synchronous rhythms in reciprocally inhibitory model neurons. Ann Rev Neurosci 1985;8:233–61.
[18] Skinner FK, Kopell N, Marder E. Mechanisms for oscillation and frequency control in reciprocally inhibitory model neural networks. J Comput Neurosci June 1994;1(1–2):69–87.
[19] Rubin J, Terman D. Geometric analysis of population rhythms in synaptically coupled neuronal networks. Neural Comput March 2000;12(3):597–645.
[20] Kopell N, Ermentrout G. Mechanisms of phase-locking and frequency control in pairs of coupled neural oscillators. Handb Dyn Syst 2002;2:3–54.
[21] Terman D, Ahn S, Wang X, Just W. Reducing neuronal networks to discrete dynamics. Physica D Nonlinear Phenomena 2008;237(3):324–38.
[22] Destexhe A, Contreras D, Sejnowski TJ, Steriade M. A model of spindle rhythmicity in the isolated thalamic reticular nucleus. J Neurophysiol 1994;72(2):803–18.
[23] Shilnikov AL, Gordon R, Belykh I. Polyrhythmic synchronization in bursting networking motifs. Chaos September 2008;18(3).
[24] Perkel DH, Mulloney B. Mechanism of postinhibitory rebound in molluscan neurons. Science 1974;185(4146):181–3.

UNCORRECTED PROOF

Please cite this article as: R. Nagornov et al., Mixed-mode synchronization between two inhibitory neurons with post-inhibitory rebound, Commun Nonlinear Sci Numer Simulat (2015), http://dx.doi.org/10.1016/j.cnsns.2015.11.024

[25] Daun S, Rubin JE, Rybak IA. Control of oscillation periods and phase durations in half-center central pattern generators: a comparative mechanistic analysis. J Comput Neurosci 2009;27(1):3–36.
[26] Angstadt JD, Grassmann JL, Theriault KM, Levasseur SM. Mechanisms of postinhibitory rebound and its modulation by serotonin in excitatory swim motor neurons of the medicinal leech. J Compar Physiol A-Neuroethol Sensory Neural Behav Physiol August 2005;191(8):715–32.
[27] Matveev V, Bose A, Nadim F. Capturing the bursting dynamics of a two-cell inhibitory network using a one-dimensional map. J Comput Neurosci 2007;23(2):169–87.
[28] Kopell N, Somers D. Rapid synchronization through fast threshold modulation. Biol Cybern 1993;68(5).
[29] Ermentrout GB, Terman DH. Piking neuron models. Single neurons, populations, plasticity. Springer; 2010.
[30] Shilnikov AL. Complete dynamical analysis of a neuron model. Nonlinear Dyn may 2012;68(3, SI):305–28.
[31] Ermentrout GB, Terman DH. Mathematical foundations of neuroscience. Cambridge University Press; 2002.
[32] Channell P, Cymbalyuk G, Shilnikov AL. Origin of bursting through homoclinic spike adding in a neuron model. Phys Rev Lett March 2007;98(13):134101.
[33] Channell P, Fuwape I, Neiman AB, Shilnikov AL. Variability of bursting patterns in a neuron model in the presence of noise. J Comput Neurosci Dec 2009;27(3):527–42.
[34] Jalil S, Allen D, Youker J, Shilnikov AL. Toward robust phase-locking in melibe swim central pattern generator models. Chaos 2013;23(4).
[35] Belykh IV, Shilnikov AL. When weak inhibition synchronizes strongly desynchronizing networks of bursting neurons. Phys Rev Lett Aug 2008;101(7):078102.
[36] Pikovsky A. A dynamical model for periodic and chaotic oscillations in the Belousov-Zhabotinsky reaction. Phys Lett A 1981;85(1):13–16.
[37] Channell P, Fuwape I, Neiman AB, Shilnikov AL. Variability of bursting patterns in a neuron model in the presence of noise. J Comp Neurosci 2009;27(3).573–543
[38] Neiman AB, Dierkes K, Lindner B, Han L, Shilnikov AL. Spontaneous voltage oscillations and response dynamics of a Hodgkin-Huxley type model of sensory hair cells. J Math Neurosci 2011;1(11).

UNCORRECTED PROOF

Please cite this article as: R. Nagornov et al., Mixed-mode synchronization between two inhibitory neurons with post-inhibitory rebound, Commun Nonlinear Sci Numer Simulat (2015), http://dx.doi.org/10.1016/j.cnsns.2015.11.024